2016 IEEE 55th Conference on Decision and Control (CDC)
ARIA Resort & Casino
December 12-14, 2016, Las Vegas, USA

A Physical Parameter-Based Skidding Model for the Snakeboard

Hadi Salman[1], Tony Dear[1], Sevag Babikian[2], Elie Shammas[2], and Howie Choset[1]

Abstract— **The physical violation of a nonholonomic system's idealized constraints in the form of skidding has recently elucidated interest in new models in order to directly incorporate the phenomenon into the system dynamics. However, such models either are too simple to capture physical attributes or have otherwise been tested only on systems with simple behaviors, such as the rolling disk. In this work, we present a novel skidding model, based on physical parameters, for a snakeboard system, which is simultaneously rich in behavior but simple in design. This model extends the system's configuration space and associates traction forces to a skidding angle using an experimentally verified observation from the literature. We validate our model in simulation and discuss its advantages over the Rayleigh dissipation function skidding model. We also show that the model accurately predicts a physical system's behavior in experimentation with tuned parameters and standard controllers.**

I. INTRODUCTION

Mechanical system models often incorporate nonholonomic constraints to represent restrictions on velocity, such as the no-slip requirement of wheels. While these constraints often lead to simpler models, for example via a reduction process, they are idealized and do not fully represent system behavior when the violation of the constraints is nontrivial. It would thus be desirable to modify the constraints to make them less rigid while maintaining their mathematical structure, but at the same time basing such modifications on physical intuition.

The phenomenon of skidding occurs when a system's wheels slip sideways and can be observed in vehicles and wheeled robots. One such wheeled system that we focus on in this paper is the snakeboard (Fig. 1), a mechanical system whose motion is governed by both kinematic constraints and dynamics [1], [2]. This system consists of two sets of wheels, each of which can rotate about the center point of an axle. To ride the snakeboard, one alternates between rotating one's torso with one's ankles to move the wheelsets. The mechanical model (Fig. 2) has a rotor situated at the center of the longitudinal axis to simulate the human rider's torso. The rotor and wheel axle angles are actuated, and the latter are nonholonomically constrained, allowing the snakeboard to locomote due to input joint actuation. Depending on its environment, the effects of skidding can be considerable for the snakeboard, as its locomotion relies heavily on the assumption that the wheels do not slip while rotating.

[1]H. Salman, T. Dear and H. Choset are with the Robotics Institute at Carnegie Mellon University, Pittsburgh, PA 15213, USA. {hadis@andrew., tonydear@, choset@cs.}cmu.edu

[2]S. Babikian, and E. Shammas are with the Department of Mechanical Engineering, American University of Beirut, Riad El Solh, Beirut, Lebanon. {sb56, es34}@aub.edu.lb

Fig. 1: A snakeboard, composed of a rigid axis and two footrests on rotating wheelsets.

A number of different ways to represent skidding and controllers based on them have been developed in previous work. De Wit and Khennouf [3] treated skidding as an unknown bounded perturbation, although the unknown parameters complicated efficient controller design [4], [5]. D'andréa-novel et al. [6] studied both skidding and slipping using singular perturbation theory, which was used by Motte and Campion [7] to derive a slow manifold controller. However, its performance was overly dependent on the ability to accurately estimate wheel stiffness. Low and Wang [8] presented a kinematic model in which different types of perturbations are classified and then geometrically related to wheel skidding and slipping. These perturbations had to be estimated and relied on real-time kinematic sensor measurements [9]–[11], which may not always be available.

Contrary to the aforementioned models, Sidek and Sarkar [12] included skidding directly in the dynamics of a two-wheeled mobile robot by relaxing the nonholonomic constraints, tracking an additional variable and adding the corresponding dissipative traction forces to the equations of motion. Bazzi et al. [13], [14] extended this work to the kinematic rolling disk, preserving the original constraint form without adding dissipative forces and allowing for reduction of the equations of motion. Separately, Dear et al. [15] considered a skidding model and motion planner [16] for the snakeboard, incorporating dynamics in addition to constraints. While this work extended previous analysis to a relatively complex system, the formulation was based on a single-parameter Rayleigh dissipation model and did not have the physical connection of [12] or [14].

In this paper, we extend the previous work and derive a skidding model for the snakeboard by tracking a new "rotational" variable in the configuration space and relating the associated dissipative force to the skidding angle through Pacejka's formula [17], inspired by Sidek and Sakar [12]. Through simulation in different conditions and comparison of results with the Rayleigh dissipation model [15], we are able to elucidate the physical interpretation of some of the parameters in the two models. We also test this model on a physical snakeboard robot, showing that skidding can be

978-1-5090-1836-9/16/$31.00 ©2016 IEEE

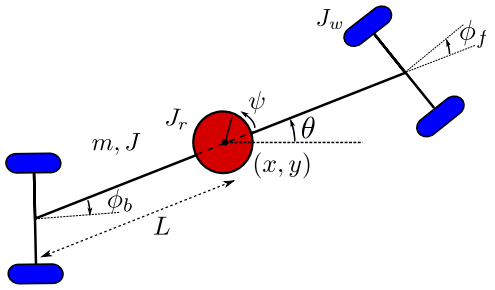

Fig. 2: The mechanical configuration of the snakeboard. Parameters include m, L, J, J_r, and J_w. The joint angle inputs are ψ and $\phi = \phi_f = -\phi_b$.

significant for certain gaits and can be well predicted by our model, as compared to the Rayleigh or ideal models.

II. THE NATURE OF SKIDDING

Skidding takes place at the level of an individual wheel, which deforms due to the lateral cornering force F generated when negotiating a turn [14], shown in Fig. 3. Alternatively, the point of contact between the wheel and the ground will have nonzero velocity, violating the assumption of zero instantaneous velocity in the ideal model. As such, the wheel's direction of travel then differs from the direction in which it is pointing by an angle δ.

A snakeboard has nonholonomically constrained wheels on both the front and back of the body. We denote the angles of these wheels with respect to the body as ϕ_f and ϕ_b, respectively. In this paper, we constrain the actuation of the two sets of wheels such that $\phi = \phi_f = -\phi_b$, so the lateral forces and offset angles on them are equal but in opposite directions. Previous work [16] has shown that removing this degree of freedom still allows for sufficient locomotion of the system in $SE(2)$, the group of planar motions, while simplifying the model's complexity. As shown in Fig. 4, the front wheels travel at an angle of $\phi - \delta$ away from the body axis. The actual velocity vector v can be seen as having components v_a in the "allowable" direction and v_s in the "forbidden" direction. This leads to a net rotation of the whole system by an angle β.

For comparison purposes, we will also refer to the Rayleigh dissipation function model [15] in order to verify the simulation results of our proposed model in this paper. This model is based on replacing the "hard" nonholonomic constraint equations, which prohibit all motion in the directions perpendicular to the wheelsets, with soft dissipative forces modeled derived from the skidding Rayleigh dissipation function

$$R_{skid} = \frac{1}{2} k_s v_s^2. \tag{1}$$

Here k_s is an empirically tuned constant reprsenting the magnitude of skidding, and v_s is the velocity in the perpendicular direction shown in Fig. 4. This dissipative function is then appended to the Euler-Lagrange equations of motion.

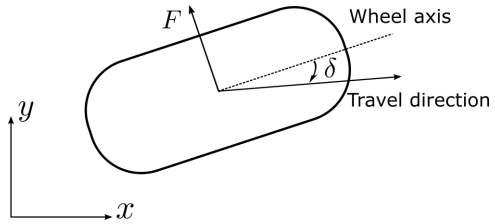

Fig. 3: The lateral force F on the wheel and the resultant deviating angle δ in the travel direction due to skidding.

III. SKIDDING AND THE SNAKEBOARD

We now specify the mathematical model of the snakeboard incorporating our proposed skidding model. The system's configuration, shown in Fig. 2, is given by coordinates $q = (x, y, \theta, \psi, \phi, \beta)^T$, where $(x, y, \theta)^T \in SE(2)$ locate the system in the world frame by denoting the global position of the center of mass at the rotor and the body's orientation with respect to the inertial x axis. The variable ψ denotes the angle of the rotor while ϕ denotes the coupled angles of the wheelsets. Finally, we add a new configuration variable β, similar to what Sidek and Sarkar [12] did for a two-wheeled nonholonomic robot, which denotes the extra rotational angle of the whole body due to the skidding effects.

The actuated variables are the rotor angle ψ and the coupled wheelset angles ϕ. The mass of the snakeboard is m centered in the middle of the rotor, while J, J_r, and J_w are the moments of inertia of the body, the rotor, and the wheelsets about an axis perpendicular to the x-y plane respectively. We will assume as in [15] that $mL^2 = J + J_r + 2J_w$ is the total inertia of the system, where the total length of the snakeboard is $2L$, and that the wheelsets are massless.

A. Equations of Motion

To derive the equations of motion of a general mechanical system, we require the Lagrangian and the mathematical form of any constraints acting on the system. The Lagrangian in this case is simply the kinetic energy of the system, written in the inertial frame as $l(q, \dot{q}) = \frac{1}{2}\dot{q}^T M(q)\dot{q}$, where $M(q)$ is the mass matrix given by

$$M(q) = \begin{pmatrix} m & 0 & 0 & 0 & 0 & 0 \\ 0 & m & 0 & 0 & 0 & 0 \\ 0 & 0 & mL^2 & J_r & 0 & mL^2 \\ 0 & 0 & J_r & J_r & 0 & J_r \\ 0 & 0 & 0 & 0 & 2J_w & 0 \\ 0 & 0 & mL^2 & J_r & 0 & mL^2 \end{pmatrix}. \tag{2}$$

Note the coupling between the new variable β and the other rotational configuration variables, θ, ψ, and ϕ, due to the nonzero terms in the last row and column of the mass matrix.

We also require the nonholonomic constraints of the system, of which there are two, one for the front and one for the back set of wheels. Accounting for the variable β, the constraint forms can be written in the Pfaffian form

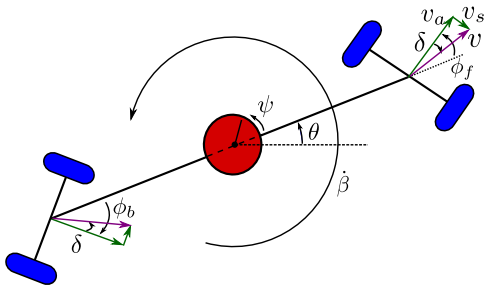

Fig. 4: A velocity component v_s in the disallowed direction is added to the component v_a in the wheel axis direction, resulting in a net velocity v and a net rotation of the entire system with velocity $\dot{\beta}$.

$A(q)\dot{q} = 0$, where

$$A(q) = \begin{pmatrix} -\sin(\theta+\phi) & -\sin(\theta-\phi) \\ \cos(\theta+\phi) & \cos(\theta-\phi) \\ L\cos\phi & -L\cos\phi \\ 0 & 0 \\ 0 & 0 \\ -L\cos\phi & L\cos\phi \end{pmatrix}^T . \quad (3)$$

As with the Lagrangian, the components associated with the original configuration velocities are identical to models derived previously; the difference here appears in the nonzero components for $\dot{\beta}$ in the last column of $A(q)$.

We are now in a position to use the Euler-Lagrange dynamics formulation to derive the equations of motion of the modified system. The general form of these equations is

$$\frac{d}{dt}\frac{\partial l(q,\dot{q})}{\partial \dot{q}} - \frac{\partial l(q,\dot{q})}{\partial q} = \tau + A(q)^T(\lambda - F). \quad (4)$$

Here, $l(q,\dot{q})$ and $A(q)$ are the Lagrangian and constraint matrix as defined above. The vector $\tau = (0,0,0,\tau_\psi,\tau_\phi,0)^T$ incorporates generalized forces or input torques on the rotor and wheels, while $\lambda = (\lambda_1,\lambda_2)^T$ are the standard Lagrange multipliers associated with the two constraints. Finally, we have an additional vector $F = (F_1,F_2)^T$ representing the dissipative traction forces on each of the wheelsets, which act opposite to the constraint forces given by λ. We will assume by symmetry that the same traction force acts on each set of wheels, or $F = F_1 = F_2$.

The constraint equations along with the Euler-Lagrange equations make up eight total equations, but we have a ninth unknown due to the addition of the traction force F. Thus in order to render our system of equations solvable, we will derive a relationship between the traction force and the configuration variables and velocities.

B. Traction Force Model

Similar to the approach taken by Sidek and Sarkar [12] for their two-wheeled mobile robot, we turn to Pacejka's magic formula [17] to derive the desired relationship. This is an elegant formula developed by curve fitting and commonly used when modeling tires. It relates the lateral force on a wheel to the skidding angle in the following manner:

$$F = D\sin(C\arctan(B\eta)) + \Delta S_v, \quad (5)$$

TABLE I: Gait inputs used in simulation

Gait	$\phi(t)$	$\psi(t)$
1	$0.3\sin(t)$	$0.5\sin(t)$
2	0.2	$0.5\cos(t)$

where

$$\eta = (1-E)(\delta + \Delta S_h) + \frac{E}{B}\arctan(B(\delta + \Delta S_h)).$$

The variable δ is the skidding angle and the coefficients B, C, D, E, ΔS_h, ΔS_v are fitting parameters dependent on the following factors:

- The load on the wheel
- The conditions of the surface of contact
- The camber angle of the wheel

The relations between the coefficients and the attributes specified can be found in Bakker et al. [17].

We will assume for the snakeboard that the distance that separates the two wheels of the same wheelset is very small and that the wheelset can be represented as one single wheel. This wheel is allowed to roll and is actuated by rotating it about an axis perpendicular to the x-y plane, for example as shown in Fig. 3. This allows us to express the lateral traction force at the center of the wheelset to the skidding angle δ.

From Fig. 4, the skidding angle δ can be written as

$$\delta = \arctan\left(\frac{v_s}{v_a}\right), \quad (6)$$

where v_s is the velocity due to skidding along the wheelset axis, and v_a is the velocity of the wheelset perpendicular to this axis (its velocity in the ideal no-skid case). These two velocities can be derived by projecting the system's velocities along the wheelset axis to obtain v_s and perpendicular to it to obtain v_a, and can be written as

$$\begin{aligned} v_s &= L\dot{\beta}\cos\phi, \\ v_a &= \dot{x}\cos(\theta+\phi) + \dot{y}\sin(\theta+\phi) + L(\dot{\theta}-\dot{\beta})\sin\phi. \end{aligned} \quad (7)$$

We can now find F in terms of the configuration velocities by combining equations (5), (6), and (7). This allows us to eliminate this unknown, and we are left with eight variables in eight equations, which can be solved numerically.

IV. SIMULATION AND RESULTS

In order to evaluate our new skidding model, we will simulate its response under certain inputs and compare the results with those of the Rayleigh dissipation function model. We numerically solve the equations of motion with the input torques determined by an inverse dynamics controller:

$$\begin{aligned} \tau_\psi &= \ddot{\psi}_d + K_d(\dot{\psi}_d - \dot{\psi}) + K_p(\psi_d - \psi), \\ \tau_\phi &= \ddot{\phi}_d + K_d(\dot{\phi}_d - \dot{\phi}) + K_p(\phi_d - \phi). \end{aligned} \quad (8)$$

Here, ψ_d and ϕ_d are the desired trajectories of the controlled variables, and K_p and K_d are the proportional and derivative gains of the controller, respectively. We experiment with two different gaits as shown in Table I. Throughout the simulations, we keep the following parameters constant:

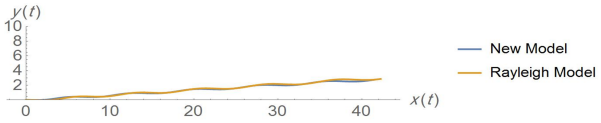

Fig. 5: The trajectories predicted by the new model and the Rayleigh model using gait 1, with load 2.54N, camber angle 0.52rad, and duration 35s.

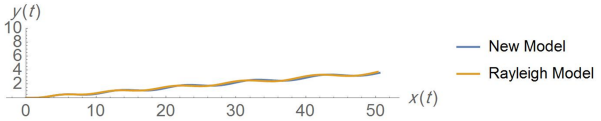

Fig. 6: The trajectories predicted by the new model and the Rayleigh model using gait 1, with load 5.08N, camber angle 0.3rad, and duration 35s.

$J_r = 4$, $J_w = 1$, $L = 4$, $K_p = 100$, and $K_d = 10$. We will vary the mass m of the snakeboard in order to study the effect of changing the load on the wheels on skidding. In doing so, the body inertia J is changed as well due to our assumption that mL^2 is related to J.

Three different simulations are conducted, all using skidding parameters corresponding to a dry asphalt road. Figs. 5 and 6 compare trajectories that result from the use of gait 1 for both the Rayleigh and the new skidding models. We vary the load and camber angles for the two scenarios as specified in the figure captions, but keep all other parameters the same in modeling a specific environment of a dry asphalt road. Fig. 7 shows the trajectories from using gait 2 but with the same conditions otherwise as the second simulation. In terms of the resultant trajectory, the first two simulations show a great agreement between the two models in terms of the overall shape and distance traveled, despite the fact that the new model has many more degrees of freedom than the Rayleigh model. The third simulation also shows qualitative similarities in terms of the shape, while the divergence between the two trajectories over time can be minimized by tuning the parameters of the new model.

A. Discussion

From the simulation results, we see that our proposed skidding model for the snakeboard is at least as powerful as the Rayleigh dissipation function model. This is not surprising, given that it has many more parameters. The advantages of this new model is that the coefficients of Pacejka's magic formula, the key relationship of this model, are empirically derived from known physical attributes. Furthermore, the model can be easily adjusted for different conditions of the system and its environment, such as the load on the wheels or the conditions of the ground [17].

In order to correlate the skidding coefficient of the Rayleigh function k_s with the parameters used in this new model, we varied the parameters and empirically swept the value of k_s to find the most similar response (in terms of the shape of the trajectory and the distance traveled) from the Rayleigh dissipation function model. We found that the

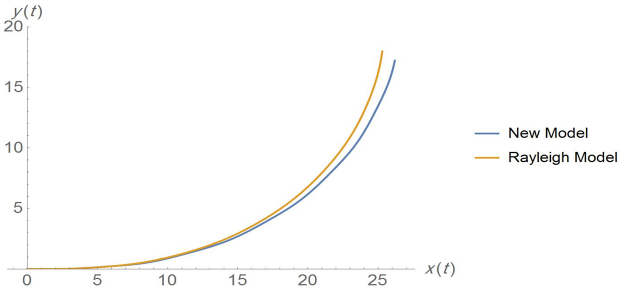

Fig. 7: The trajectories predicted by the new model and the Rayleigh model using gait 2, with load 5.08N, camber angle 0.3rad, and duration 35s.

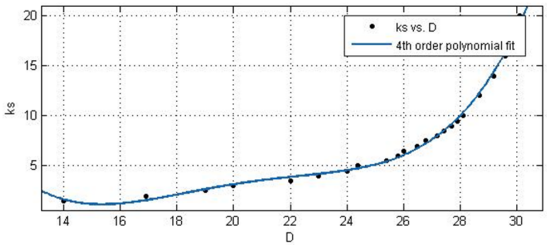

Fig. 8: 4th-order polyomial curve fitting for the Rayleigh coefficient k_s as a function of the skidding parameter D.

Rayleigh model is unable to reproduce simulation results for certain load values, no matter the camber angle. This confirms the extended flexibility of Pacejka's parameters.

On the other hand, we noticed that by fixing all the parameters and changing only the D parameter, we are able to reproduce the same results of the Rayleigh model in varying the value of k_s. Since D has been shown to be only dependent on road conditions [17], we can say the same for the Rayleigh model. Fig. 8 shows a 4th-order polynomial curve fitting between the two parameters, which correspond quite well within reasonable ranges of both. If the parameter D were to remain constant and the other parameters varied, for example due to different load values or camber angles, we observe different results, some of which are unobtainable with the Rayleigh model alone. This fact is verified through some experiments in the next section.

V. EXPERIMENTATION ON SNAKEBOARD

To verify that our proposed model is physically valid, we conduct experiments using a snakeboard developed by the Vision and Robotics Laboratory at the American University of Beirut. Shown in Fig. 9, this snakeboard has a flywheel that rotates in the center and two sets of steering friction wheels that are situated at opposite ends of the robot. These components are controlled by DC motors, and the same sinusoidal gaits used in simulation can be replicated on the robot here, with the motions of the two wheelsets being synchronized according to our earlier assumption. The robot is also supported by caster wheels to hold up the robot, but these do not constrain the robot's motion as they are free to rotate.

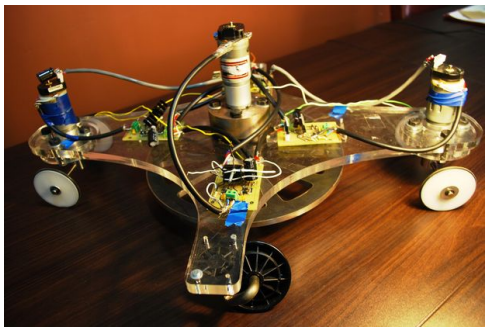

Fig. 9: The snakeboard that we used for experimentation.

TABLE II: Simulation parameters for the snakeboard

System	Value	Skidding	Value
m	7.00	B	0.09
J	0.41	C	2.00
J_r	0.0238	D	1.00
J_w	0.001	E	0.60
L	0.25	ΔS_v	0.0
		ΔS_h	0.0

For our experiments, we command the proposed gaits to the robot's motors and record the resultant trajectories using a Vicon motion capture system. We also take the estimated system parameters for the physical system, along with the skidding parameters that are tuned starting with values from the literature [13], [14] as shown in Table II, and simulate the predicted behavior with the same starting conditions. This gives us a way to evaluate the validity of the skidding model in contrast with the ideal and Rayleigh models. For the following comparisons, we consider the Rayleigh model with large k_s ($k_s > 60$ for this system) to be effectively identical to the ideal model, since any motion in the skidding direction is damped out on a very small timescale.

In the first experiment, we execute the forward gait shown in Table III. The result is shown in blue solid in Fig. 11, with the heading direction substantially different from the Rayleigh model predictions; the traveled distance is also much less than that predicted by the ideal model (black dot-dashed). In contrast, the experimental trajectory agrees more closely with the new skidding model (dark red dashed) in both average heading and displacement. These results show that the effects of skidding are nontrivial, particularly because of the friction generated with the continuous oscillation of the wheels. More importantly, we conclude here that compared to the parameter-based model, the Rayleigh model has less predictive fidelity for the true trajectory of the snakeboard for any value of k_s. The value of this parameter, which dictates how fast the skidding motions are damped out, only affects the total distance traveled, whereas the average heading remains the same for all values of k_s. This can be seen in the three simulated trajectories for different values of k_s in Fig. 11.

Next we consider a "rotate-in-place" gait, which was specifically derived for the snakeboard by Ostrowski et al. [1]. An example of what this gait does is shown in Fig. 10. With minimal displacements in the x and y directions,

TABLE III: Inputs for the experimental gaits

Gait	$\phi(t)$	$\psi(t)$
Forward	$0.916\sin(4t)$	$1.570\sin(4t)$
Rotate	$0.916\sin(2t)$	$1.570\sin(4t)$

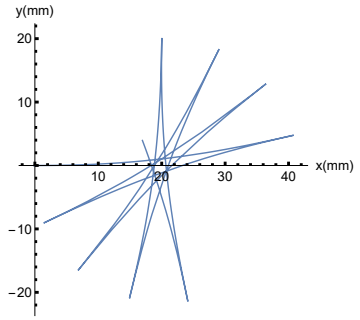

Fig. 10: The resultant workspace trajectory of the "rotate-in-place" gait.

the snakeboard is able to reorient itself incrementally. The specific joint trajectories used to achieve this are shown in Table III, the key feature being that the frequency of the rotor is twice that of the wheelsets.

For this gait, the experimental result is shown in blue solid in Fig. 12. The absolute angle rotated in 14 seconds is almost the same (about 0.95 rad) as predicted by both the new model (red dashed) and the closest Rayleigh model with $k_s = 9$ (black dot-dashed), and is in accordance with the experimental result. However, the parameter-based model is able to predict the actual trajectory shape more closely than its predecessor. From visual inspection, it would appear that the experimental trajectory has about two frequency components, while the Rayleigh prediction only has one. As shown in Fig. 13, other values of k_s only gives us a less accurate prediction of the final rotation angle, and furthermore it still does not get us the correct frequency profile of the trajectory. We therefore conclude that, as with the forward gait, the parameter-based model is both more powerful and more faithful to the actual system dynamics when compared to the simpler Rayleigh model.

A separate observation is that the simulation of the rotate gait is much closer to the experimental trajectory compared to the two for the forward gait. We hypothesize that this is due to not including wheel slip in our model, which occurs in the wheel longitudinal direction as opposed to skidding in the lateral and would have a higher impact on forward motion. We plan to verify this in future work.

VI. CONCLUSIONS AND FUTURE WORK

In this paper, we proposed a new skidding model for the snakeboard, based on the physical effects of the system in its environment. Inspired by an earlier simpler model for skidding on a two-wheeled mobile robot [12], we presented a novel skidding model that accounts for skidding in a mixed dynamic system by adding a rotational variable to the configuration space and incorporating lateral traction forces into the equations of motion using Pacejka's magic formula.

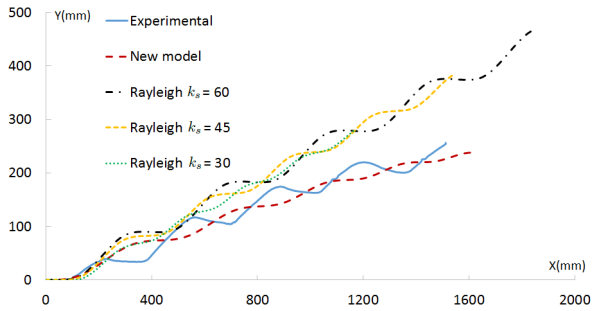

Fig. 11: Comparison between the experimental, new, and the Rayleigh models for the forward gait (duration 7.7s). The experimental trajectory is closer to that of the new model than any of the Rayleigh simulations for different k_s values.

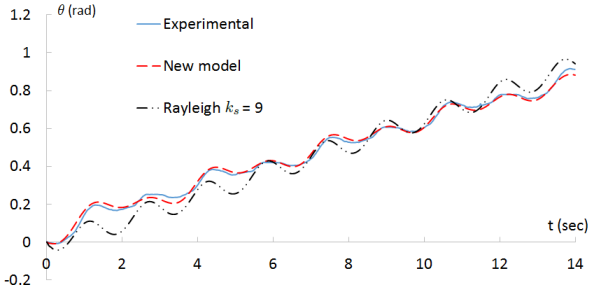

Fig. 12: Comparison between the experimental, new, and the Rayleigh models for the rotate gait (duration 14s). The experimental trajectory is closer to that of the new model than the closest Rayleigh simulation with $k_s = 9$.

By simulating the system under different conditions and with different gaits, we were able to compare the results to those of the Rayleigh dissipation function model and comment on the relationships between the two. Finally, we ran some gaits on the snakeboard and showed that in general skidding effects can be quite substantial and can be well predicted by our model, as compared to the Rayleigh or ideal models.

In future work, we may want to explore whether the effects of wheel slip, as opposed to wheel skid, are prominent for physical systems as well; these two concepts were explored together in simulation using Rayleigh functions by Dear et al. [15]. It would also be worthwhile to study these effects under more elaborate trajectories that do not necessarily involve gaits, but hybrid and differential flatness-based motion planners instead [16]. Finally, we would like to continue extending this work to a more general analysis of skidding in nonholonomic systems, in particular using the reduced geometric framework that has elucidated much of the understanding of these systems in the first place.

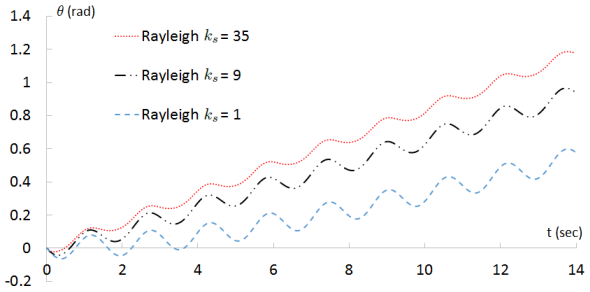

Fig. 13: Rayleigh model trajectories for different k_s values for the rotate gait. The frequency and phase of the trajectories remain roughly the same for each.

References

[1] J. Ostrowski, J. Burdick, A. D. Lewis, and R. M. Murray, "The mechanics of undulatory locomotion: The mixed kinematic and dynamic case," in *Robotics and Automation, 1995. Proceedings., 1995 IEEE International Conference on*, vol. 2. IEEE, 1995, pp. 1945–1951.

[2] E. A. Shammas, H. Choset, and A. A. Rizzi, "Towards a unified approach to motion planning for dynamic underactuated mechanical systems with non-holonomic constraints," *The International Journal of Robotics Research*, vol. 26, no. 10, pp. 1075–1124, 2007.

[3] C. C. De Wit and H. Khennouf, "Quasi-continuous stabilizing controllers for nonholonomic systems: Design and robustness considerations," in *Proceedings of the 3rd European Control Conference*, 1995, pp. 2630–2635.

[4] M. Corradini, T. Leo, and G. Orlando, "Robust stabilization of a mobile robot violating the nonholonomic constraint via quasi-sliding modes," in *American Control Conference, 1999. Proceedings of the 1999*, vol. 6. IEEE, 1999, pp. 3935–3939.

[5] M. L. Corradini, T. Leo, and G. Orlando, "Experimental testing of a discrete-time sliding mode controller for trajectory tracking of a wheeled mobile robot in the presence of skidding effects," *Journal of robotic systems*, vol. 19, no. 4, pp. 177–188, 2002.

[6] B. D'andréa-novel, G. Campion, and G. Bastin, "Control of wheeled mobile robots not satisfying ideal velocity constraints: a singular perturbation approach," *International Journal of Robust and Nonlinear Control*, vol. 5, no. 4, pp. 243–267, 1995.

[7] I. Motte, G. Campion, *et al.*, "A slow manifold approach for the control of mobile robots not satisfying the kinematic constraints," *IEEE Transactions on Robotics and Automation*, vol. 16, no. 6, pp. 875–880, 2000.

[8] D. Wang and C. B. Low, "Modeling and analysis of skidding and slipping in wheeled mobile robots: control design perspective," *Robotics, IEEE Transactions on*, vol. 24, no. 3, pp. 676–687, 2008.

[9] C. B. Low and D. Wang, "Integrated estimation for wheeled mobile robot posture, velocities, and wheel skidding perturbations," in *Robotics and Automation, 2007 IEEE International Conference on*. IEEE, 2007, pp. 2355–2360.

[10] ——, "Gps-based path following control for a car-like wheeled mobile robot with skidding and slipping," *Control Systems Technology, IEEE Transactions on*, vol. 16, no. 2, pp. 340–347, 2008.

[11] ——, "Gps-based tracking control for a car-like wheeled mobile robot with skidding and slipping," *Mechatronics, IEEE/ASME Transactions on*, vol. 13, no. 4, pp. 480–484, 2008.

[12] N. Sidek and N. Sarkar, "Dynamic modeling and control of nonholonomic mobile robot with lateral slip," in *Systems, 2008. ICONS 08. Third International Conference on*. IEEE, 2008, pp. 35–40.

[13] S. Bazzi, E. Shammas, and D. Asmar, "Novel modeling of skidding effects on the nonholonomic motion of a vertical rolling disk," in *Advanced Robotics (ICAR), 2013 16th International Conference on*. IEEE, 2013, pp. 1–6.

[14] ——, "A novel method for modeling skidding for systems with nonholonomic constraints," *Nonlinear Dynamics*, vol. 76, no. 2, pp. 1517–1528, 2014.

[15] T. Dear, S. D. Kelly, M. Travers, and H. Choset, "Snakeboard motion planning with viscous friction and skidding," in *Robotics and Automation (ICRA), 2015 IEEE International Conference on*. IEEE, 2015, pp. 670–675.

[16] T. Dear, R. L. Hatton, M. Travers, and H. Choset, "Snakeboard motion planning with local trajectory information," in *ASME 2013 Dynamic Systems and Control Conference*. American Society of Mechanical Engineers, 2013, pp. V002T33A002–V002T33A002.

[17] E. Bakker, L. Nyborg, and H. B. Pacejka, "Tyre modelling for use in vehicle dynamics studies," SAE Technical Paper, Tech. Rep., 1987.